Journal of Directed Energy, **2**, Fall 2006, 119–132

Compact, Optically Guided, Megawatt Free-Electron Laser Amplifier for Maritime Propagation

Phillip Sprangle, Joseph Peñano,* and Bahman Hafizi[1]

Plasma Physics Division, Naval Research Laboratory, Washington, D.C. 20375

We present a conceptual design and parameters for a compact, megawatt-class, optically guided, free-electron laser (FEL) amplifier. Full-scale laser propagation simulations, including the effects of aerosols, turbulence, and thermal blooming, indicate that operating the FEL in water vapor transmission windows (i.e., 1.045, 1.625, and 2.141 μm) can result in high propagation efficiencies in a maritime environment (>50% over a 5-km range). In the present design we choose the FEL wavelength to be 2.141 μm because of propagation and generation advantages as well as for eye safety reasons. The average output power of this high-gain FEL amplifier is ~1.5 MW, and the input is provided by a low-average-power (<50-W) FEL oscillator. Diffractive spreading of the FEL output beam is sufficiently large to allow the first grazing angle relay mirror to be close to the exit of the wiggler without exceeding the mirror damage intensity threshold level, which is taken to be 50 kW/cm^2. In this design the wiggler length is <2 m and, depending on the mirror grazing angle and the optical beam quality, the distance from the wiggler exit to the relay mirror can be <3 m.

KEYWORDS: Free-electron laser amplifier, Maritime propagation, Optical guiding

1. Introduction

The free-electron laser (FEL) is capable of producing high average power at high efficiency without the conventional thermal management and waste issues associated with other laser systems.[18] In addition, the operating wavelength can be tuned for optimized propagation in a maritime environment.[22] These unique features make the FEL a leading candidate for naval directed energy applications.[6,14,15,21]

Propagation of high-power laser beams in the atmosphere involves a complex, linear and nonlinear interaction between various physical processes. The theoretical/numerical model used in this study includes the effects of aerosol and molecular scattering, aerosol heating and vaporization, thermal blooming due to aerosol and molecular absorption, atmospheric turbulence, and beam quality. These processes are modeled in a fully three-dimensional and time-dependent manner. It is found that aerosols, which consist of water, sea salt, organic matter, dust, soot, biomass smoke, urban pollutants, etc., are particularly important because they result in laser scattering, absorption, and enhanced thermal blooming.

In this paper we present parameters for a conceptual design of a compact, megawatt-class, optically guided, FEL amplifier. There are a number important characteristics and

Received February 18, 2006; revision received June 15, 2006.

*Corresponding author; e-mail: joseph.penano@nrl.navy.mil.

[1]Icarus Research, Inc., P.O. Box 30780, Bethesda, MD 20824-0780.

advantages of the proposed configuration. In an optically guided FEL amplifier the filling factor, i.e., the ratio of the electron beam to the optical beam cross-sectional area, remains relatively constant throughout the wiggler region, and the radiation amplitude increases exponentially until saturation. The FEL efficiency can be increased by tapering the wiggler. Alternatively, in a uniform wiggler, enhanced efficiency can be obtained by frequency detuning the input signal. The optical beam upon exiting the wiggler can be pinched by focusing the electron beam with external focusing fields. The Rayleigh range of the pinched optical beam can be short. As a result the first relay mirror can be placed close to the wiggler without exceeding the intensity damage threshold. The first relay mirror is a grazing incidence reflector. For the power levels of interest we choose the FEL wavelength to be 2.141 μm because of propagation and generation advantages as well as for eye safety reasons.

Recently a high-gain FEL amplifier operating in the optically guided regime was experimentally demonstrated at the Brookhaven National Laboratory.[13] Our analysis of this experiment is in close agreement with the experimental results and will be discussed in more detail in Sec. 4.

2. Laser Propagation in a Maritime Environment

The optimum wavelength for efficient high-energy laser (HEL) propagation depends on the atmospheric conditions and a number of interrelated physical processes that include thermal blooming due to aerosol and molecular absorption,[19] turbulence,[11] aerosol and molecular scattering,[12] thermal scattering due to heated aerosols, and aerosol heating and vaporization.[1,5,7,27] The relative importance of these processes depends on the parameters of the atmospheric environment, which can vary significantly depending on location and time.

Atmospheric environments contain various types and concentrations of aerosols. Aerosols can absorb laser energy and conductively heat the surrounding air, resulting in an increase in thermal blooming of the HEL beam.[4,22] In general, aerosols consist of hygroscopic and nonhygroscopic particles of various sizes and chemical compositions. Oceanic aerosols consist of sea salt, water, and organic material. Nonhygroscopic aerosols are composed of dust, soot, biomass smoke, and other carbon-based compounds. These aerosols typically have much larger absorption coefficients than water-based aerosols. While they are normally present in continental, rural, and urban environments, dust aerosols can also be present in maritime environments hundreds of miles from shore.[17]

2.1. Maritime atmosphere model

The Advanced Navy Aerosol Model (ANAM) is used to model the near-surface maritime environment.[26] The ANAM aerosol distribution is composed of various modes that represent aerosols of different compositions and sizes. These aerosol modes will absorb laser energy and vaporize at different rates. The aerosol size distribution function

$$F(R,t) = \sum_{j=0}^{4} F_j(R,t),$$

where R is the aerosol radius, is represented as a superposition of five "modes," with each mode representing aerosols with a particular physical composition and origin. The complex refractive index values for the various aerosol modes were obtained from Ref. 10. However, preliminary experiments[9] performed at the Naval Research Laboratory indicate that the

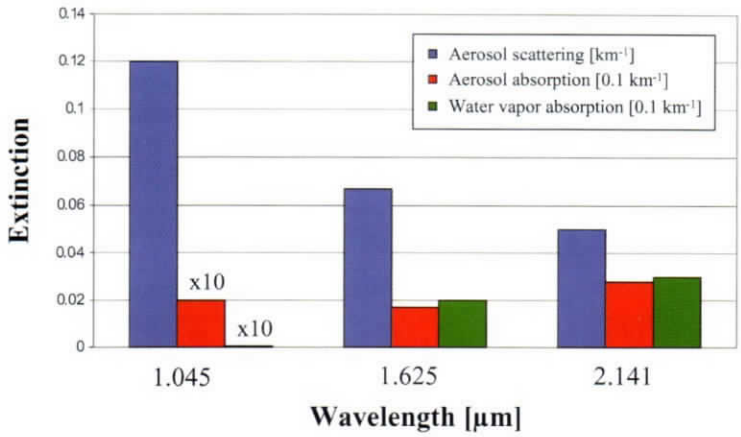

Fig. 1. Aerosol scattering, aerosol absorption, and water vapor (molecular) absorption coefficients used for the model maritime environment of the propagation simulation. Aerosol scattering and absorption are calculated using ANAM; water vapor absorption is calculated using MODTRAN4.

absorption of seawater aerosols may be significantly less than reported in Ref. 10. The aerosol distribution can evolve with time, due to vaporization, for example. The aerosol absorption and scattering coefficients are also time dependent. Mode 0 represents dust particles of continental origin, mode 1 represents water-soluble aerosols, and modes 2–4 represent marine aerosols (sea salt and water) that result from different processes.

We use MODTRAN to calculate the molecular absorption and scattering coefficients.[2] Figure 1 plots the gross scattering and absorption coefficients due to aerosol and molecular contributions in the water vapor transmission windows, $\lambda = 1.045$, 1.625, and 2.141 μm. The gross scattering and absorption coefficients that we obtain are comparable with in situ measurements.[3,8]

2.2. HEL propagation simulations

To simulate HEL propagation we use the High Energy Laser Code for Atmospheric Propagation, HELCAP,[22,23] developed at the Naval Research Laboratory. HELCAP includes the effects of 1) aerosol and molecular scattering, 2) aerosol heating and vaporization, 3) thermal blooming due to both aerosol and molecular absorption, 4) atmospheric turbulence, and 5) laser beam quality, i.e., all of the effects discussed in the preceding section. It is the first HEL propagation model that integrates all these physical processes in a fully three-dimensional, time-dependent manner. In modeling the aerosol effects, we account for the aerosol distribution and the various aerosol modes (water-based, dust, soot, etc.).

In HELCAP the laser electric field is represented as

$$\boldsymbol{E} = A(x, y, z, t)\exp[i(\omega z/c - \omega t)]\hat{\boldsymbol{e}}_x/2 + \text{c.c.},$$

where $\omega = 2\pi c/\lambda$ is the laser frequency, $\hat{\boldsymbol{e}}_x$ is a unit polarization vector in the x direction, $A(x, y, z, t)$ is the complex laser amplitude, and the laser intensity is $I = cAA^*/8\pi$. HELCAP solves a nonlinear Schrödinger-like equation that has the form

$$\frac{\partial A}{\partial z} = \frac{ic}{2\omega}\nabla_\perp^2 A + \left[i\frac{\omega}{c}(\delta n_T + \delta n_{\text{TB}}) - \frac{1}{2}(\alpha + \beta)\right]A,$$

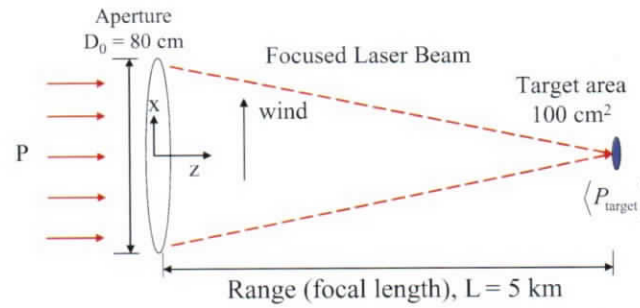

Fig. 2. Schematic of laser and target configuration used in the full-scale propagation simulations.

where $\alpha = \alpha_m + \alpha_A$ is the total absorption coefficient, $\beta = \beta_m + \beta_A$ is the total scattering coefficient, and δn_T and δn_{TB} denote the refractive index variation due to atmospheric turbulence and thermal blooming, respectively; $\alpha_m(\alpha_A)$ is the molecular (aerosol) absorption coefficient; $\beta_m(\beta_A)$ is the molecular (aerosol) scattering coefficient. The quantities δn_T, δn_{TB}, α, and β are space and time dependent and determined self-consistently in the presence of aerosol heating and vaporization.

In what follows, we simulate the propagation of a pulsed FEL beam. The pulse train is characterized by pulses of 1-ps duration separated by 1 ns. For a beam with 1 MW of average power, the peak power of each pulse is 1 GW. The peak intensity of the pulse, among other factors, determines the amount of nonlinear self-focusing due to the optical Kerr effect. However, it is the average intensity of the pulse train that determines thermal blooming.

The transmitted power at the source is denoted by P, and the laser is focused onto a remote target at a range of 5 km (Fig. 2). The target is taken to be circular with an area of 100 cm^2. The propagation direction is along the z axis, and a uniform transverse wind, with velocity $V_W = 5$ m/s, is directed along the y axis. Atmospheric turbulence is modeled by a Kolmogorov spectrum with structure constant $C_n^2 = 10^{-15}\ \text{m}^{-2/3}$. The pointing jitter associated with the laser beam is taken to have an angular spread of 2 μrad and a white noise temporal spectrum. The detailed atmospheric parameters used for these simulations are presented in Ref. 22.

Figure 3 plots the time-averaged power on target versus the transmitted power P for the three wavelengths of interest. The time average is performed over the dwell time of 1 s. Our results show that for a maritime environment, the optimum wavelength depends on the transmitted power. For $P < 1.5$ MW, propagation is mostly affected by aerosol scattering and the average power on target increases with P. In this regime, the 1.625- and 2.141-μm wavelengths provide slightly greater power on target than the 1.045-μm wavelength. This is due to the lower aerosol scattering coefficient associated with the longer wavelengths. For $P < 1.5$ MW, the propagation efficiency is roughly 50% for the three wavelengths considered. For example, $P = 1$ MW results in $\langle P_{\text{target}} \rangle \sim 0.55$ MW for $\lambda = 1.625$ and 2.141 μm. However, for $P > 1.5$ MW, thermal blooming becomes important. In this high-power regime the optimum wavelength is 1.045 μm due to the lower molecular absorption coefficient in that water vapor window. For $P = 3$ MW, $\langle P_{\text{target}} \rangle \sim 1$ MW for 1.045 μm while $\langle P_{\text{target}} \rangle \sim 0.8$ MW for 1.625 and 2.141 μm.

For the power levels of interest, i.e., $P \leq 1.5$ MW average power, the FEL wavelength is chosen to be 2.141 μm. For maritime propagation there is no distinct advantage in operating

Table 1. Wiggler parameters

Parameter	Value
Wiggler field B_W	5 kG
Wiggler parameter K	1.86
Period λ_w	4 cm
Length L_w	1.5 m

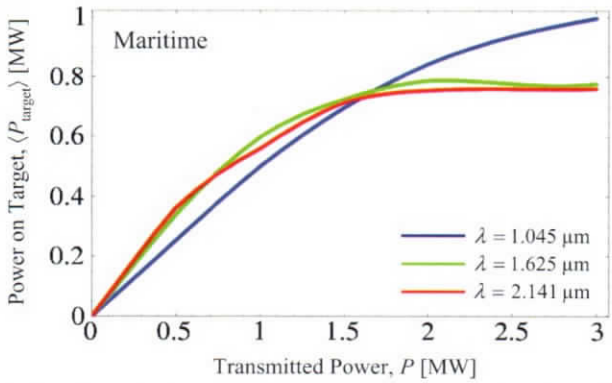

Fig. 3. Time-averaged power on target $\langle P_{\text{target}} \rangle$ versus transmitted power P in a maritime environment for the wavelengths $\lambda = 1.045$, 1.625, and 2.141 μm. The time average is performed over a dwell time of 1 s. Initial beam profile has $R_0 = 50$ cm, $D_0 = 80$ cm. Simulation geometry is shown in Fig. 2. Target range $L = 5$ km; beam focus = 5 km; target area = 100 cm^2; wind speed $V_W = 5$ m/s; turbulence strength $C_n^2 = 10^{-15}$ m$^{-2/3}$; pointing jitter angular amplitude = 2 μrad (white noise).

the FEL at either 1.045 or 1.625 μm. In the following section, we present design parameters for a high-gain FEL amplifier operating at 2.141 μm capable of achieving ~1.5 MW of average output power. We note that for the intensity levels achievable in the present HEL systems, it is the average power, not the peak power, that determines the propagation and lethality characteristics of the HEL beam.

3. Optically Guided FEL Amplifier Operating at 2.141 μm

Using the Source Dependent Expansion (SDE) formulation,[25] expressions for the optical growth rate, wave number shift, spot size, and optical curvature of the optical beam in an FEL amplifier are obtained in the Appendix. These results are used to design a compact megawatt FEL in the optically guided, high-gain regime, i.e., one having a matched optical spot size. In addition, focusing the electron beam at the wiggler exit is shown to result in a pinched optical beam with a shortened Rayleigh range. A schematic diagram of the FEL amplifier configuration is shown in Fig. 4. Finally, it is shown that by frequency detuning the FEL, efficiency can be more than doubled. The following discussion is based on the design parameters listed in Tables 1 and 2 and for the case of no frequency detuning.

Table 2. Electron beam parameters

Parameter	Value
Energy E_b	81 MeV
Current I_b	1 kA
Radius R_b	0.02 cm
Normalized emittance $\varepsilon_{n,\mathrm{rms}}$	15 mm-mrad
Duty factor D	1.5×10^{-3}
RF linac frequency	750 MHz
Micropulse duration	2 ps
Betatron wavelength $\lambda_B = 2\gamma\lambda_w/K$	7 m

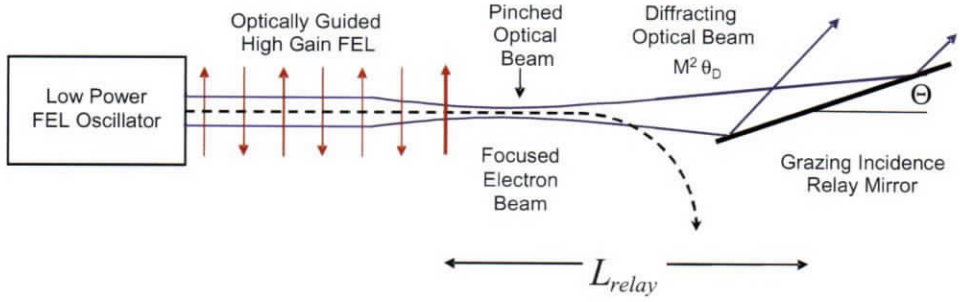

Fig. 4. Schematic of high-gain FEL amplifier with a grazing relay mirror. The input signal can be obtained using a low-average-power FEL oscillator. The radiation beam is optically guided in the wiggler and optically pinched at the exit. The pinched optical beam has a shortened Rayleigh range and undergoes rapid diffraction upon exiting the wiggler. By employing a grazing incidence configuration, the resultant footprint on the relay mirror can be made sufficiently large to avoid damage.

3.1. Operating wavelength

In the present design the resonant operating wavelength of a linearly polarized optical beam is $\lambda = \lambda_w(1 + K^2/2)/2\gamma^2 = 2.141\ \mu$m, where $\gamma = E_b[\mathrm{MeV}]/0.511 + 1$ is the total relativistic mass factor (Tables 1 and 2).

3.2. Gain length

The power gain length in the optically guided regime, in the absence of frequency detuning ($\Delta\omega = 0$), is

$$L_e = 1/2\Gamma = \frac{\lambda_w}{8\pi}\left[\frac{(2+3f)}{2(1+2f)^2}\left(\frac{\nu}{\gamma}\right)^{1/2}\frac{K}{\sqrt{1+K^2/2}}\right]^{-1} = 14\,\mathrm{cm}, \qquad (1)$$

where $f = R_b^2/R_L^2 \leq 1$ is the filling factor, $\nu = I_b[\mathrm{kA}]/17$ is Budker's parameter, I_b is the electron beam current in kiloamperes, $K = qB_W\lambda_w/2\pi mc^2 = 1.9$ is the wiggler strength parameter, $B_W = 5$ kG is the wiggler field, and $\lambda_w = 4$ cm is the wiggler period. The transverse

profiles of the optical and electron beam are Gaussian with radii R_L and R_b, respectively [see Eqs. (A2) and (A4)].

3.3. FEL efficiency

In the optically guided, high-gain regime the efficiency of conversion from electron beam power to optical power is given by[21,24]

$$\eta = \frac{\lambda_w \Delta k}{2\pi} = \frac{f^{1/2}(2+3f)^{1/2}}{(1+2f)^2}\left(\frac{v}{\gamma}\right)^{1/2}\frac{K}{\sqrt{1+K^2/2}} = 0.8\%. \tag{2}$$

Here, Δk is the wave number shift, defined in Eq. (A3). Equation (2) represents the intrinsic efficiency in the absence of electron beam recirculation. FEL efficiency can be increased by tapering the wiggler[15,16,24] or by frequency detuning.[21,24]

3.4. Optical guiding

The FEL optical beam can undergo refractive guiding within the wiggler. An envelope equation for the optical beam spot size can be obtained by using the results in the Appendix, and the condition for a matched optical beam can be obtained. For optical guiding, the power gain length is nearly equal to the free-space Rayleigh range, that is,

$$L_e = \frac{(2+3f)^{1/2}}{2f^{1/2}(1+2f)} Z_R, \tag{3}$$

where $Z_R = \pi R_L^2/\lambda = 22$ cm is the Rayleigh range. The optical guiding condition in Eq. (3) can be rewritten in terms of the beam current:

$$I_b[\mathrm{kA}] = 1.1 \times 10^{-2}\frac{f^3(1+2f)^6}{(2+3f)^3}\left(\frac{\lambda_w}{R_b}\right)^4\frac{\left(1+K^2/2\right)^3}{\gamma^3 K^2} = 1\,\mathrm{kA}. \tag{4}$$

In addition, the centroid of the FEL optical beam can be steered by gradually bending the electron beam.

3.5. Saturated peak and average optical power

The peak optical power at saturation is $P = \eta I_b V_b = 1\,\mathrm{GW}$, where $V_b = 81\,\mathrm{MV}$ is the electron beam voltage. The average power at saturation is

$$\langle P\rangle = \eta D I_b V_b = 1.5\,\mathrm{MW}, \tag{5}$$

where $D = 1.5 \times 10^{-3}$ is the duty factor and $\eta = 1.2\%$ ($\Delta\omega/\omega = -1.5\%$).

3.6. Electron pulse slippage (lethargy)

In the high-gain regime, electron slippage (lethargy) is shown to be significantly less than in the low-gain regime and is not a concern for this design. The slippage length, i.e., the separation between the optical and electron pulse, is $S \equiv (v_g - v_z)L_w/c$, where $v_g = \partial\omega/\partial k$ is the optical pulse group velocity, $v_z \cong c(1 - 1/2\gamma_z^2)$ is the axial electron beam velocity, and $\gamma_z = \gamma/\sqrt{1+(K^2/2)}$. Making use of the high-gain FEL dispersion relation,[21,24] the

group velocity is $v_g \cong c[1 - 1/3\,\gamma_z^2 - (\lambda/\pi R_L)^2/2]$, and the slippage length is

$$S = \lambda N_w \left[\frac{1}{3} - \left(\frac{\lambda\gamma_z}{\pi R_L}\right)^2\right] \leq 27\,\mu\text{m}, \tag{6}$$

where $N_w = L_w/\lambda_w$ is the number of wiggler periods. The well-known slippage length in the low-gain regime is λN_w. Slippage in the high-gain regime is reduced by more than a factor of three.

3.7. Pinched optical beam

The intensity on the first relay mirror must be below a damage threshold level. To further reduce the intensity on the mirror, the optical beam can be pinched at the wiggler exit in order to shorten the Rayleigh range.[15,21] By employing external focusing fields near the wiggler exit, the electron beam and in turn the optical beam can be pinched. By making use of grazing incidence geometry, the intensity on the mirror can be further reduced.

The spot size ($1/e$ Gaussian field radius) of the optical beam, $R_L(z)$, is obtained by solving Eqs. (A5), (A6), and (A8). The radius of the electron beam is denoted by $R_b(z)$. Figure 5 plots $R_L(z)$ and $R_b(z)$ as functions of the propagation distance z. The entrance to the wiggler is at $z = 0$ and extends to $z = L_w = 1.5$ m. In Fig. 5a the radius of the electron beam is constant and the optical beam is guided through the wiggler with a constant spot size. Upon exiting the wiggler, the optical beam diffracts. In the example of Fig. 5b the electron beam is focused by external fields applied near the wiggler exit. This pinches the optical beam and as a result, the optical beam diffracts more rapidly than in the unpinched example.

3.8. Optical beam quality and beam spreading

It is common practice to characterize the higher order modal content of a laser beam by a beam quality parameter denoted by M^2. The quantity $M^2 \geq 1$ is a "times diffraction-limited" parameter that, for a fundamental Gaussian beam, is unity. Upon exiting the FEL interaction region, i.e., wiggler, the spatial spreading of the optical beam is given by

$$W^2(z) \equiv \frac{2}{P}\int_0^\infty r^2 I(r,z) 2\pi r\,dr = W_o^2 + M^4\theta_D^2(z - L_w)^2, \tag{7}$$

where W is the laser beam spot size, P is the power, and I is the intensity. In Eq. (7), W_o is the minimum spot size at $z = L_w$, $\theta_D = \lambda/(\pi W_o)$ is the diffraction (spreading) angle of an ideal Gaussian beam, and M^2 is a measure of the beam quality. For a nonideal optical beam the diffraction angle is $M^2\theta_D$ at the exit of the wiggler. Using the paraxial wave equation in Sec. 2, it can be shown that the general expression for the evolution of M^2 is

$$M^2(z) = \left(\frac{4\pi^2}{P^2}\left\{\left(\int_0^\infty Ir^3\,dr\right)\int_0^\infty\left[\left(\frac{\partial I^{1/2}}{\partial r}\right)^2 + \left(\frac{\partial\phi}{\partial r}\right)^2 I\right] r\,dr - \left(\int_0^\infty I\frac{\partial\phi}{\partial r}r^2\,dr\right)^2\right\}\right)^{1/2}, \tag{8}$$

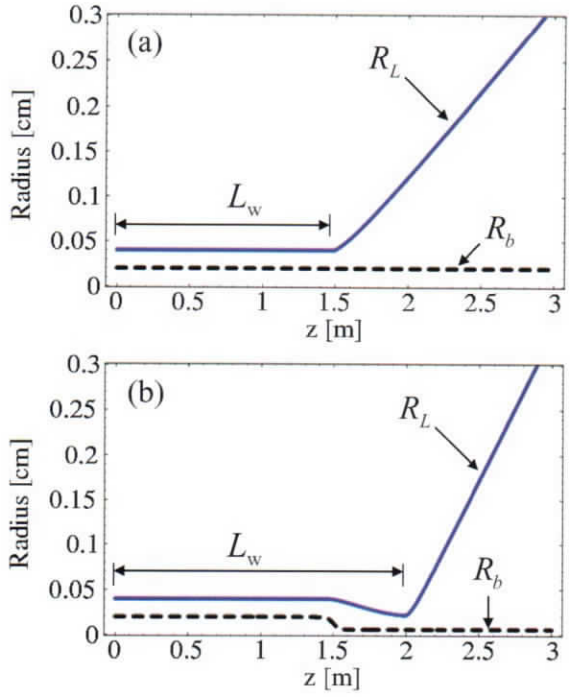

Fig. 5. Plots of optical beam radius (R_L) and electron beam radius (R_b) versus propagation distance z. Wiggler entrance is at $z = 0$, and the exit is at $z = L_w \sim 1.5$ m. The FEL operates in the high-gain regime, in which the optical beam maintains a constant spot size by optical guiding. Outside the wiggler the optical beam diffracts and spreads transversely, as indicated in panel a. By focusing the electron beam at the wiggler exit the optical beam can be pinched down to $R_{L,\text{pinch}} = 0.21$ mm, as indicated in panel b. The pinched optical beam diffracts more rapidly compared to the unpinched example, i.e., has a shorter Rayleigh range, $Z_{R,\text{pinch}} = \pi R^2_{L,\text{pinch}}/\lambda = 6.7$ cm. In generating this figure a frequency detuning of $\Delta\omega/\omega = -1.5\%$ was used.

where the complex laser amplitude has been expressed in terms of the intensity I and phase ϕ as $A \sim I^{1/2}(r, z)\exp[i\phi(r, z)]$. When the laser beam propagates in a region of uniform refractive index, i.e., outside of the wiggler, M^2 is constant. Simulations using the FEL code MEDUSA indicate that the beam quality of an optically guided FEL beam is fairly good. For parameters similar to those in Table 1 and 2, simulation results indicate the $M^2 \approx 1.5$ at the exit of the wiggler.[20]

3.9. Distance between first relay mirror and wiggler

To avoid damage, the distance between the wiggler and relay mirror must exceed

$$L_{\text{relay}} = \frac{Z_R}{M^2}\left(\frac{\langle I\rangle}{\langle I_{\text{damage}}\rangle}\right)^{1/2}\sin^{1/2}\Theta, \tag{9}$$

Table 3. FEL optical beam parameters for operating wavelength $\lambda = 2.141\ \mu$m

Parameter	Values	
Frequency detuning $\Delta\omega/\omega$	0	−1.5%
Spot size in wiggler R_L	0.33 mm	0.4 mm
Filling factor, f	0.36	0.25
Rayleigh range (unpinched, at wiggler exit) Z_R	16 cm	23 cm
Gain length (power) L_e	14 cm	14 cm
Efficiency (uniform wiggler) η	0.77%	1.2 %
Average intensity (unpinched, at wiggler exit) $\langle I \rangle$	0.53 GW/cm^2	0.58 GW/cm^2
Pinched laser spot size $R_{L,\,\mathrm{pinch}}$	0.17 mm	0.21 mm
Rayleigh range (pinched, at wiggler exit) $Z_{R,\mathrm{pinch}}$	4 cm	6.7 cm
Average pinched intensity $\langle I_{\mathrm{pinch}} \rangle$	2.2 GW/cm^2	2.1 GW/cm^2
Peak output power P	0.63 GW	1 GW
Average output power $\langle P \rangle$	1 MW	1.5 MW
Number of power e-folds L_w/L_e	10.6	10.5
Average input power $\langle P_{\mathrm{input}} \rangle$	43 W	40 W
Optical beam quality M^2	1.5	1.5

Table 4. First relay mirror parameters (for $\Delta\omega/\omega = -1.5\%$)[a]

Parameter	Values	
Tilt angle Θ, deg	45	5
Distance from wiggler (unpinched) L_{relay}, m	14	5
Distance from wiggler (pinched) L_{relay}, m	8	3

[a]The average intensity damage threshold was taken to be $\langle I_{\mathrm{damage}} \rangle = 50\ \mathrm{kW/cm^2}$.

where Θ is the tilt angle (Fig. 4), $Z_R = \pi R_L^2/\lambda$ is the Rayleigh range at the exit of the wiggler, $\langle I \rangle = 2\langle P \rangle/\pi R_L^2$ is the average intensity at exit of the wiggler, and $\langle I_{\mathrm{damage}} \rangle = 50\,\mathrm{kW/cm^2}$ is the average intensity damage threshold of the mirror. Using the parameters in Tables 1–3, we obtain, for an unpinched optical beam,

$$L_{\mathrm{relay}} = \begin{cases} 15\,\mathrm{m}, & \Theta = 45\,\mathrm{deg} \\ 8\,\mathrm{m}, & \Theta = 5\,\mathrm{deg} \end{cases}, \tag{10}$$

and for a pinched beam,

$$L_{\mathrm{relay}} = \begin{cases} 5\,\mathrm{m}, & \Theta = 45\,\mathrm{deg} \\ 3\,\mathrm{m}, & \Theta = 5\,\mathrm{deg} \end{cases}. \tag{11}$$

as summarized in Table 4.

3.10. Frequency detuning and efficiency enhancement

In an FEL the efficiency can be increased by operating at a frequency that is detuned from the resonant value $\omega_R = 2\pi c/\lambda$. In general, however, operating off-resonance leads to a reduction in the growth rate.[18] If the operating frequency is denoted by ω, the modification to the present analysis is the replacement of the wave number shift Δk with $\Delta k - (\omega - \omega_R)/(2c\gamma_z^2)$ in the expression for the efficiency in Eq. (2) and in Eq. (A7), which leads to the dispersion relation. Note that the left-hand side of Eq. (A8) is not changed.

4. Discussion and Conclusions

Conceptual design parameters for a compact megawatt-class FEL amplifier operating in the optically guided, high-gain regime are presented. The design presented here assumes that the FEL amplifier is driven by a high-quality RF linac-generated electron beam. Optical guiding allows the interaction length to be sufficiently long to achieve substantial growth of the input signal. Electron pulse slippage, which can limit the FEL interaction length, is shown to be significantly reduced for a high-gain amplifier. By pinching the optical beam at the wiggler exit, the Rayleigh range is shortened, thus reducing the required distance to the first relay mirror. The optical beam can be pinched by focusing the electron beam with external magnetic fields or by utilizing the betatron oscillation of the electron beam envelope. Grazing incidence geometry permits a further reduction in intensity to avoid damage to the mirror.

In this design the operating wavelength, 2.141 μm, is chosen because of propagation and generation advantages as well as for eye safety reasons. For a 1-kA, 81-MV electron beam, a wiggler field of 5 kG, and a frequency detuning of -1.5%, the power gain length is 14 cm, the intrinsic efficiency is $\sim$1.2%, the optical output power is 1 GW, and the average output power is 1.5 MW, assuming a duty factor of 1.5×10^{-3} for the RF linac. Focusing the electron beam radius down by a factor of $\sim$3 at the exit of the $\sim$1.5-m wiggler reduces the optical beam Rayleigh range by a factor of $\sim$4. Depending on the mirror grazing angle and the optical beam quality, the distance from the wiggler exit to the first relay mirror can be $<$3 m. The length of the optical system, which includes the amplifier section and the first relay mirror, can be $<$5 m.

A recent experiment at the Brookhaven National Laboratory (BNL) has demonstrated the optically guided, high-gain FEL amplifier concept. This experiment utilized a 10-m-long wiggler and an S-band RF linac that produced a 100-MeV, 300-A electron pulse of radius 0.2 mm. The wiggler period and strength parameter were 3.9 cm and 1.1, respectively. Experiments showed optical guiding in a high-gain FEL amplifier operating at $\lambda = 0.8\ \mu$m using a Ti-sapphire laser as the seed. Dipole steering magnets located along the wiggler were used to deflect the electron beam by $\sim$1 mrad, and the light beam was shown to be steered and guided by the electron beam. The transverse profile of the optically guided light beam was shown to be less than half the size of an unguided diffracting light beam. The power peak output power was $\sim$150 MW (Ref. 13). Our simulations of the BNL experiment predict a power e-folding length of 42 cm, a guided spot size of 0.24 mm ($1/e$ of intensity), and a peak power output of $\sim$180 MW, in close agreement with the experimental results.

Simulations of the FEL amplifier, taking into account emittance, energy spread, and nonuniformity of the optical guiding due to variation of the electron current within the pulse, are required to fully evaluate the present design. Also, while estimates indicate that a modest external magnetic field is sufficient to focus the beam, more refined analysis is

required to design the pinch region of the wiggler. In the absence of optical pinching, the distance to the first relay mirror can be <10 m.

5. Acknowledgments

This work was sponsored by the Joint Technology Office and the Office of Naval Research.

Appendix

The source-dependent expansion (SDE) formulation[25] can be used to analyze the dynamics of the optical beam in FELs. A summary of the principal SDE equations is given in this Appendix. For a planar wiggler, the electric field of the radiation can be taken to be linearly polarized and given by

$$E(r, z) = \tfrac{1}{2} A(r, z) \exp[i\omega(z/c - t)] + \text{c.c.} \tag{A1}$$

For the fundamental Gaussian mode, the complex envelope $E_o(r, z)$ is written as

$$A(r, z) = A_o \exp[i\Psi(z)] \exp\left\{-[1 - i\alpha(z)]r^2 / R_L^2(z)\right\}, \tag{A2}$$

where A_o is the amplitude on axis,

$$\Psi(z) = \int_0^z [\Delta k(z') - i\Gamma(z')]\, dz', \tag{A3}$$

$\Delta k(z)$ is the wave number shift, $\Gamma(z)$ is the spatial growth rate, $\alpha(z)$ is related to the curvature of the optical wavefronts, and $R_L(z)$ is the spot size of the beam. To allow for an electron beam with a radius $R_b(z)$ that varies along the propagation axis, the electron beam density is taken to be

$$n_b(z, r) = n_b(0)\left[R_b^2(0)/R_b^2(z)\right] \exp\left[-r^2/R_b^2(z)\right]. \tag{A4}$$

The SDE equations for the spot size and $\alpha(z)$ are given by[21]

$$\frac{dR_L(z)}{dz} - \frac{2c\alpha(z)}{\omega} \frac{1}{R_L(z)} = -H_I(z) R_L(z), \tag{A5}$$

$$\frac{d\alpha(z)}{dz} - \left[\frac{2c}{\omega}\right] \frac{1 + \alpha^2(z)}{R_L^2(z)} = 2[H_R(z) - \alpha(z) H_I(z)], \tag{A6}$$

respectively. Here,

$$H(z) = 4 \frac{\nu}{\gamma} \frac{c}{\omega} \left(\frac{K^2 k_w^2}{1 + K^2/2}\right) \frac{1}{R_b^2(z)} \frac{f(z)}{[1 + 2f(z)|^2} \frac{1}{|\Delta k(z) - i\Gamma(z)]^2}, \tag{A7}$$

where $\nu = I_b[\text{kA}]/17$ is Budker's parameter, $k_w = 2\pi/\lambda_w$, $f(z) = R_b^2(z)/R_L^2(z)$ is the filling factor, and the subscripts R and I denote real and imaginary parts. The final SDE equation for the phase shift and growth rate is given by

$$\Delta k(z) - i\Gamma(z) + \left(\frac{c}{\omega}\right) \frac{[1 + \alpha^2(z)]}{R_L^2(z)} - i \frac{[1 - i\alpha(z)]}{R_L(z)} \frac{dR_L(z)}{dz} + \frac{1}{2} \frac{d\alpha(z)}{dz}$$
$$= -[1 + 2f(z)] H(z). \tag{A8}$$

Equations (A5), (A6), and (A8) describe the optical beam in the high-gain FEL amplifier. The electron beam can be focused to produce a pinched optical beam.

References

[1]Armstrong, R.L., Appl. Optics **23**, 148 (1984); Armstrong, R.L., J. Appl. Phys. **56**, 2142 (1984); Armstrong, R.L., S.A.W. Gerstl, and A. Zardecki, J. Opt. Soc. Am. A **2**, 1739 (1985).

[2]Berk, A., G.P. Anderson, P.K. Acharya, J.H. Chetwynd, L.S. Bernstein, E.P. Shettle, M.W. Matthew, and S.M. Adler-Golden, "MODTRAN4 User's Manual," Air Force Research Laboratory, Hanscom Air Force Base, MA (2000).

[3]Bodhaine, B.A., J. Geophys. Res. **100**, 8967 (1995); Quinn, P.K., D.J. Coffman, T.S. Bates, E.J. Welton, D.S. Covert, T.L. Miller, J.E. Johnson, S. Maria, L. Russell, R. Arimoto, C.M. Carrico, M.J. Rood, and J. Anderson, J. Geophys. Res. **109**, D19S01 (2004).

[4]Brown, R.T., and D.C. Smith, J. Appl. Phys. **46**, 402 (1975).

[5]Caledonia, G.E., and J.D. Teare, J. Heat Transfer **99**, 281 (1977).

[6]Colson, W.B., A. Todd, and G.R. Neil, "A High Power Free Electron Laser Using a Short Rayleigh Length," *Free Electron Lasers 2001*, edited by M. Brunken, H. Genz, and A. Richter, Holland: Elsevier Science, 2002, pp. II-9–II-10; Blau, J., V. Bouras, A. Kalfoutzos, G. Allgaier, T. Fontana, P.P. Crooker, and W.B. Colson, Nucl. Instrum. Methods Phys. Res. A **507**, 44 (2003).

[7]Davies, S.C., and J.R. Brock, Appl. Opt. **26**, 786 (1987).

[8]Doss-Hammel, S., D. Tsintikidis, D. Merritt, and J. Fontana, Proc. SPIE **5552**, 208 (2004).

[9]Fischer, R.P., A. Ting, G. DiComo, J. Prosser, A. Kao, P. Sprangle, J.R. Penano, B. Hafizi, A.J.R. Bauer, D.M. Sonnenfroh, M. Shinn, and G. Neil, "High-Energy laser Propagation in a Maritime Environment," 8th Annual Directed Energy Symposium, Lihue, HI, Nov. 14, 2005.

[10]*Handbook of Geophysics and the Space Environment*, edited by A. D. Jursa, Air Force Geophysical Laboratory, Air Force Systems Command (1985).

[11]*The Infrared and Electro-Optical Systems Handbook*, vol. 2, edited by F.G. Smith, Environmental Research Institute of Michigan, Ann Arbor, MI, and SPIE Optical Engineering Press, Bellingham, WA (1993).

[12]Measures, R.M., *Laser Remote Sensing, Fundamentals and Applications*, Krieger, Malabar, FL (1992).

[13]Murphy, J., Private Communication (2005); X.J. Wang, "Megawatt Class FEL Amplifier Experiments at the NSLS SDL," presented at the Directed Energy Professional Society Symposium, Lihue, HI, Nov. 2005.

[14]Neil, G.R., C.L. Bohn, S.V. Benson, G. Biallas, D. Douglas, H.F. Dylla, R. Evans, J. Fugitt, A. Grippo, J. Gubeli, R. Hill, K. Jordan, G.A. Krafft, R. Li, L. Merminga, P. Piot, J. Preble, M. Shinn, T. Siggins, R. Walker, and B. Yunn, Phys. Rev. Lett. **84**, 662 (2000).

[15]Nguyen, D.C., and H.P. Freund, Nucl. Instrum. Methods Phys. Res. A **507**, 120 (2003); Nguyen, D.C., S.S. Kurennoy, L.M. Young, and H.P. Freund, J. Directed Energy 1, 171 (2004).

[16]Orzechowski, T.J., B.R. Anderson, J.C. Clark, W.M. Fawley, A.C. Paul, D. Prosnitz, E.T. Scharlemann, S.M. Yarema, D.B. Hopkins, A.M. Sessler, and J.S. Wurtele, Phys. Rev. Lett. **57**, 2172 (1986).

[17]Reid, J.S., D.L. Westphal, R.M. Paulus, S. Tsay, and A. van Eijk, "Preliminary Evaluation of the Impacts of Aerosol Particles on Laser Performance in the Coastal Marine Boundary Layer," NRL/MR/7534–04-8803, Naval Research Laboratory, Monterey, CA, June 2004.

[18]Roberson, C.W., and P. Sprangle, Phys. Fluids B **1**, 3 (1989).

[19]Smith, D.C., Proc. IEEE **65**, 1679 (1977).

[20]Sprangle, P., "A Compact Optically Guided Pinched Megawatt Class FEL," Eighth Annual Directed Energy Symposium, Lihue, HI, Nov. 14–18, 2005.

[21]Sprangle, P., B. Hafizi, and J. Peñano, J. Quant. Elec. **40**, 1739 (2004).

[22]Sprangle, P., J.R. Peñano, and B. Hafizi, "Optimum Wavelength and Power for Efficient Laser Propagation in Various Atmospheric Environments," NRL Technical Memorandum NR/MR/6790-05-8907 (2005).

[23]Sprangle, P., J. R. Peñano, A. Ting, B. Hafizi, and D.F. Gordon, J. Directed Energy **1**, 73 (2003); Sprangle, P., J.R. Peñano, and B. Hafizi, Phys. Rev. E **66**, 046418 (2002); Peñano, J.R., P. Sprangle, B. Hafizi, A. Ting, D.F. Gordon, and C.A. Kapetanakos, Phys. Plasmas **11**, 2865 (2004); Sprangle, P., J.R. Peñano, A. Ting, B. Hafizi, and D.F. Gordon, J. Directed Energy **1**, 73 (2003).

[24]Sprangle, P., C.M. Tang, and W.M. Manheimer, Phys. Rev. A **21**, 302 (1980); Sprangle, P., C.M. Tang, and C.W. Roberson, Nucl. Instrum. Methods Phys. Res. A **239**, 1 (1985).

[25]Sprangle, P., A. Ting, and C.M. Tang, Phys. Rev. Lett. **59**, 202 (1987).

[26]van Eijk, A.M.J., and L.H. Cohen, "The ANAM-3.0 Development," TNO Physics and Electronics Laboratory, June 2005; Piazzola, J., M.J. van Eijk, and G. de Leeuw, Opt. Eng. **39**, 1620 (2000).

[27]Williams, F.A., Int. J. Heat Mass Transfer **8**, 575 (1965).

The Authors

Dr. Bahman Hafizi received B.Sc. and Ph.D. degrees in physics from Imperial College, London, in 1974 and 1978. He is president of Icarus Research, Inc. He was previously a Research Associate in the Department of Astro-Geophysics at the University of Colorado and a Staff Scientist for SAIC. His research areas include propagation of ultraintense laser pulses, laser-driven electron accelerators, laser–plasma interactions, nonlinear optics, advanced sources of electromagnetic radiation with application to imaging, lithography, and remote sensing. He is an Associate of the Royal College of Science and a member of the American Physical Society, the European Physical Society, and the IEEE.

Dr. Joseph R. Peñano received B.S. and Ph.D. degrees in plasma physics from the University of California, Los Angeles, in 1991 and 1998. He joined the NRL Beam Physics Branch in 2001. He conducts research on atmospheric propagation of ultrashort, high-intensity laser pulses for directed energy weapons and electronic countermeasure applications, advanced radiation sources, and laser-driven particle accelerators. He is the chief developer of HELCAP (High Energy Laser Code for Atmospheric Propagation). Prior to joining NRL, he held a National Research Council postdoctoral fellowship. He received the NRL Alan Berman Publication Award in 2003.

Dr. Phillip Sprangle received his Ph.D. in applied physics from Cornell University in 1973. He is Chief Scientist and Head of the Beam Physics Branch at NRL. His research areas include atmospheric laser propagation, free-electron lasers, and laser acceleration physics. Dr. Sprangle is a fellow of the American Physical Society, the IEEE, and the DEPS. He won the International Free Electron Laser Prize (1991), E.O. Hulburt Science and Engineering Award (1986), and Sigma Xi Pure Science Award (1994), as well as numerous publication awards. He has published more that 200 refereed scientific articles (28 letters) and holds 12 U.S. invention patents.